In-Situ Imaging of Ionic Crystal Dissolution Using an Integrated Electrochemical/AFM Probe

Julie V. Macpherson,[†] Patrick R. Unwin,*[,†] Andrew C. Hillier,[‡] and Allen J. Bard*[,‡]

Contribution from the Department of Chemistry, University of Warwick, Coventry, United Kingdom CV4 7AL, and Department of Chemistry and Biochemistry, University of Texas at Austin, Austin, Texas 78712

Received March 14, 1996[⊗]

Abstract: The kinetics and mechanism controlling dissolution from the (100) cleavage face of potassium bromide single crystals in acetonitrile solutions have been identified using a novel integrated electrochemical/AFM probe and a scanning electrochemical microscope (SECM). With both techniques, dissolution is induced by perturbing the dynamic dissolution/growth equilibrium at the crystal/solution interface through the electrochemical oxidation of bromide ions. SECM measurements demonstrate that the dissolution reaction is diffusion-limited under the experimental conditions, suggesting that the surface reaction is characterized by a rate constant in excess of 5 cm s^{-1} (assuming a first-order dissolution process). The topography of the dissolving surface has been imaged in situ, under conditions which closely mimic those of the SECM measurements, using an electrochemically active AFM probe. These studies provide the first direct experimental evidence of the operation of the spiral mechanism in the dissolution of an ionic single crystal, in which steps of unit cell height unwind from screw dislocations emerging on the crystal surface.

Introduction

Dissolution and crystallization processes that occur at solid/liquid interfaces are of key importance in a wide variety of chemical reactions.[1] Scanning probe microscopy[2] has provided unprecedented kinetic and structural information on the elementary steps involved in these processes, particularly on the roles of atomic level surface features such as terrace, ledge, and kink sites.[3] Scanning tunnelling microscopy (STM)[4] and atomic force microscopy (AFM)[5] have been used to investigate dissolution reactions at both electrically conducting[6−8] and insulating surfaces.[9−18] When the substrate is conducting, dissolution can be potentiostatically controlled by connecting the sample as an electrode and monitoring topographical surface reactivity as a function of the applied potential or current.[6−8] For insulating surfaces, precise control of the interfacial undersaturation, which promotes the dissolution process, is more difficult to achieve. Initial work in this area concentrated on *ex-situ* imaging of reacted surfaces.[9] To date, the most advanced studies of dissolution activity at insulating materials have employed AFM to monitor topographical changes (at the nanometer level) on a crystal surface in real time as an undersaturated solution is flowed over a crystal face.[10−15] Local dissolution rates have been deduced by measuring the velocity of individual steps or groups of steps.[9,11,13,16,17] Such studies have allowed a direct assessment of the validity of classical theories,[19,20] which treat crystal growth and dissolution processes in terms of the movement of monatomic steps across a surface. However, the range of accessible systems has been limited to those involving low interfacial dissolution fluxes to avoid significant dissolution during image acquisition.

[†] University of Warwick.

[‡] University of Texas at Austin.

[⊗] Abstract published in *Advance ACS Abstracts,* July 1, 1996.

(1) For reviews see, for example: (a) Unwin, P. R.; Macpherson, J. V. *Chem. Soc. Rev.* **1995**, *24*, 109. (b) Macpherson, J. V.; Unwin, P. R. *Prog. React. Kinet.* **1995**, *20,* 185. (c) Blum, A. E.; Lasaga, A. In *Aquatic Surface Chemistry;* Stumm, W., Ed.; Wiley: New York, 1989; p 255. (d) Heimann, R. B. *Crystals: Growth, Properties and Applications;* Springer-Verlag: Berlin, 1982. (e) *Biological Mineralization and Demineralization*; Nancollas, G. H., Ed.; Springer-Verlag: Berlin, 1982.

(2) See, for example: (a) Snyder, S. R.; White, H. S. *Anal. Chem.* **1992**, *64,* R116. (b) Wiesendanger, R. *Scanning Probe Microscopy and Spectroscopy*; Cambridge University Press: Cambridge, UK, 1994. (c) *Scanning Tunneling Microscopy and Related Methods;* Behm, R. J., Garcia, N., Rohrer, H., Eds.; NATO ASI Series; Kluwer: The Netherlands, 1990; Vol. 184.

(3) Tiller, W. A. *The Science of Crystallization: Microscopic Interfacial Phenomena;* Cambridge University Press: New York, 1991.

(4) (a) Binnig, G.; Rohrer, H.; Gerber, C.; Weibel, E. *Phys. Rev. Lett.* **1982**, *49*, 57. For reviews see, for example: (b) *Scanning Tunneling Microscopy and Spectroscopy: Theory, Techniques and Applications;* Bonnell, D. A., Ed.; VCH: New York, 1993, and references therein. (c) Binnig, G.; Rohrer, H. *IBM J. Res. Dev.* **1986**, *30,* 355.

(5) (a) Binnig, G.; Quate, C. F.; Gerber, C. *Phys. Rev. Lett.* **1986**, *56*, 930. (b) For reviews see, for example: Quate, C. F. *Surf. Sci.* **1994**, *299*, 980. Louder, D. R.; Parkinson, B. A. *Anal Chem.* **1995**, *67*, 297A.

(6) (a) Suggs, D. W.; Bard, A. J. *J. Am. Chem. Soc.* **1994**, *116*, 10725. (b) Suggs, D. W.; Bard, A. J. *J. Phys. Chem.* **1995**, *99*, 8349. (c) Kaji, K.; Yau, S. L.; Itaya, K. *J. Appl. Phys.* **1995**, *78*, 5727. (d) Oppenheim, I. C.; Trevor, D. J.; Chidsey, C. E. D.; Trevor, P. L.; Sieradzki, K. *Science* **1991**, *254*, 687. (e) Wu, Y. C.; Pickering, H. W.; Gregory, D. S.; Geh, S.; Sakurai, T. *Surf. Sci.* **1991**, *246*, 468.

(7) Hillier, A. C.; Ward, M. D. *Science* **1994**, *263*, 1261.

(8) Carter, P. W.; Hillier, A. C.; Ward, M. D. *J. Am. Chem. Soc.* **1994**, *116*, 944.

(9) Gratz, A. J.; Manne, S.; Hansma, P. K. *Science* **1991**, *251*, 1343.

(10) Hillner, P. E.; Manne, S.; Gratz, A. J.; Hansma, P. K. *Geology* **1992**, *20*, 359.

(11) Hillner, P. E.; Manne, S.; Gratz, A. J.; Hansma, P. K. *Ultramicroscopy* **1992**, *42−44*, 1387.

(12) Manne, S.; Cleveland, J. P.; Stucky, G. D.; Hansma, P. K. *J. Cryst. Growth* **1993**, *130*, 333.

(13) Kipp, S.; Lacmann, R.; Schneeweiss, M. A. *J. Cryst. Growth* **1994**, *141*, 291.

(14) Bosbach, D.; Rammensee, W. *Geochim. Cosmochim. Acta* **1994**, *58*, 84.

(15) Bosbach, D.; Jordan, G.; Rammensee, W. *Eur. J. Mineral.* **1995**, *7*, 267.

(16) Prohaska, T.; Friedbacher, G.; Grasserbauer, M. *Fresenius' J. Anal. Chem.* **1994**, *349*, 190.

(17) Hall, C.; Cullen, D. C. *AIChE J.* **1996**, *42*, 232.

(18) Putnis, A.; Junta-Rosso, J. L.; Hochella, M. F. *Geochim. Cosmochim. Acta* **1995**, *59,* 4623.

(19) Burton, W. K.; Cabrera, N.; Frank, F. C. *Phil. Trans. R. Soc. London* **1951**, *A243*, 299.

(20) Hirth, J. P.; Pound, G. M. *J. Chem. Phys.* **1957**, *26,* 1216.

S0002-7863(96)00842-6 CCC: $12.00

The scanning electrochemical microscope (SECM)[21,22] has also proved very useful as a technique for investigating the dissolution characteristics of electrically insulating materials, in particular ionic single crystal surfaces.[23−27] With this technique, a tiny electrode (of micrometer dimensions) placed close to a crystal surface amperometrically drives and monitors the dissolution process of interest by creating a local undersaturation at the crystal/solution interface. This approach has several attributes: (i) mass transfer is well-defined and calculable; (ii) mass-transfer rates are sufficiently high to facilitate the quantitative study of fast surface reactions;[24,26] (iii) the extent of dissolution can be controlled by varying the potential applied to the probe and the period of application, allowing dissolution reactions to be switched on and off with a time scale down to the millisecond domain;[24] and (iv) the dissolution process can be initiated and monitored from targeted regions of a surface with a resolution approaching the active probe diameter, enabling the relationship between surface structure and reactivity to be investigated at the micrometer level.[24,25]

Although SECM studies have provided valuable quantitative information on local dissolution rates, important complementary topographical information has been limited to microscopic studies of reacted surfaces at a resolution on the micrometer scale, either ex situ using optical microscopy[24−26] or in situ using SECM in the negative feedback mode.[24] In this paper we describe a significant advance in the measurement of dissolution kinetics through the introduction of a complementary AFM technique in which a Pt-coated, electrochemically-active AFM tip is used to measure the topography of a dissolving crystal surface while simultaneously inducing dissolution electrochemically under conditions which closely mimic those for SECM kinetic measurements. This approach allows kinetic and structural information to be linked more closely.

The proposed approach is illustrated through studies of dissolution from the (100) cleavage face of KBr single crystals in acetonitrile solutions. This material has previously been imaged by AFM in air[16] and in ultrahigh vacuum[28] and is characterized by flat terraces, separated by steps of unit cell height, often over a scale of micrometers. Consequently, this surface has also attracted attention as a substrate for imaging adsorbates.[29] However, to the best of our knowledge, KBr surfaces have not been examined by AFM when in contact with a solution. In the studies described here, dissolution is induced electrochemically by perturbing the dynamic dissolution/growth equilibrium at the crystal/solution interface through the oxidation of bromide to tribromide. The current, monitored in the SECM configuration as a function of time and tip−substrate distance, provides information on the dissolution rate, while in-situ topographical measurements with the electrochemically active AFM tip allow the structural changes that accompany the dissolution process to be identified.

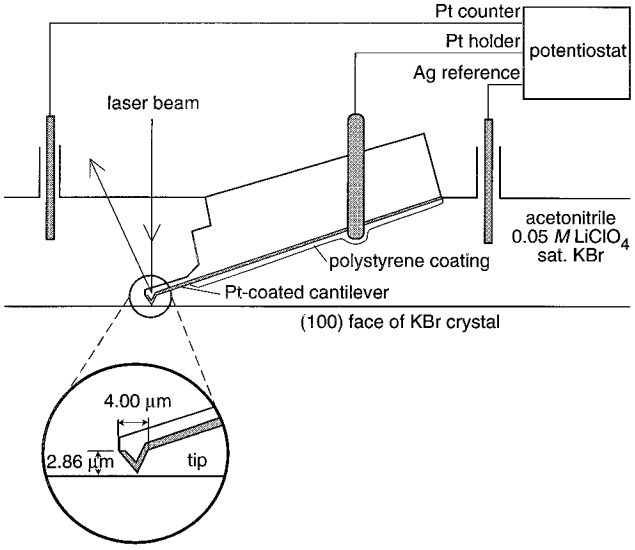

Figure 1. Schematic of the integrated electrochemical/AFM probe employed in the fluid cell.

Experimental Section

SECM Instrumentation. SECM measurements were made in a two-electrode arrangement with a home-constructed ultramicroelectrode (UME), with a radius, *a*, of 2.5, 5.0, or 12.5 μm as the working electrode and with a silver wire as a quasi-reference electrode (AgQRE). The instrumentation for SECM measurements of crystal dissolution rates was as described previously.[23−26] Dissolution was initiated and monitored at the UME by stepping the electrode potential from open circuit to +1.3 V, where the oxidation of bromide to tribromide occurred at a diffusion-controlled rate. The resulting current−time behavior was recorded as a function of tip−substrate separation. Care was taken in setting the final potential to ensure that further oxidation of tribromide to bromine, which occurs at a higher potential, did not take place. SECM-induced dissolution behavior under the latter conditions will be described elsewhere.[30]

Integrated Electrochemical/AFM Instrumentation. AFM experiments utilized a Nanoscope III scanned probe microscope and fluid cell (Digital Instruments, Santa Barbara, CA). A schematic of the cell geometry is shown in Figure 1. The AFM was equipped with a sample scanner allowing a maximum scan range of 14 μm × 14 μm, but images were generally acquired over an area of 7 μm × 7 μm. AFM probes (Nanoprobe, Park Scientific, Sunnyvale, CA) consisted of silicon nitride cantilevers (length, 200 μm; spring constant, 0.06 N/m) with integrated pyramidal tips, which had a height of 2.86 μm and a base width of 4 μm. The entire cantilever and support was sputter-coated first with a Cr anchor (100 Å) and then Pt (300 Å). A thicker Pt layer would induce a bend in the cantilever and prevent the laser diode-detection system of the AFM from being properly aligned. After the Pt-coated AFM probe had been secured in place in the cell, the underside was coated in a 1:40 (by mass) solution of polystyrene/1,2-dichloroethane solution (Aldrich, ACS reagent, Milwaukee, WI), using a fine paintbrush. This procedure served to electrically insulate the part of the probe holder that came into contact with the solution and most of the area surrounding the cantilever and tip. The coating was allowed to dry in air for 30 min. Electrical contact was made to the cantilever via the metal tip holder.

Electrochemical control of the AFM probe was effected in a three-electrode mode using a PAR 173 potentiostat and 175 programmer. The Pt-coated AFM probe served as the working electrode along with an AgQRE and a Pt counter electrode, both placed in the outlet of the fluid cell. Linear sweep voltammograms for Br^- oxidation in acetonitrile, recorded at the AFM probe, indicated that the typical electro-

(21) For reviews see, for example: (a) Bard, A. J.; Fan, F.-R. F.; Pierce, D. T.; Unwin, P. R.; Wipf, D. O.; Zhou, F. *Science* **1991**, *254*, 68. (b) Bard, A. J.; Fan, F.-R. F. *Faraday Discuss.* **1992**, *94*, 1. (c) Arca, M.; Bard, A. J.; Horrocks, B. R.; Richards, T. C.; Treichel, D. A. *Analyst* **1994**, *119*, 719. (d) Bard, A. J.; Fan, F.-R. F.; Mirkin, M. V. In *Electroanalytical Chemistry*; Bard, A. J., Ed.; Marcel Dekker: New York, 1993; Vol. 18, p 243.

(22) Bard, A. J.; Fan, F. F-R.; Kwak, J.; Lev, O. *Anal. Chem.* **1989**, *61*, 132.

(23) Macpherson, J. V.; Unwin, P. R. *J. Phys. Chem.* **1995**, *99*, 14824.

(24) Macpherson, J. V.; Unwin, P. R. *J. Phys. Chem.* **1995**, *99*, 3338.

(25) Macpherson, J. V.; Unwin, P. R. *J. Phys. Chem.* **1994**, *98*, 11764.

(26) Macpherson, J. V.; Unwin, P. R. *J. Phys. Chem.* **1994**, *98*, 1704.

(27) Macpherson, J. V.; Unwin, P. R. *J. Chem. Soc., Faraday Trans.* **1993**, *89*, 1883.

(28) Giessibl, F. J.; Binnig, G. *Ultramicroscopy* **1992**, *42*, 281.

(29) (a) Nakajima, N.; Kageshima, M.; Ara, N.; Yoshimira, M.; Kawazu, A. *Appl. Phys. Lett.* **1993**, *62*, 1892. (b) Yase, K.; Ara, N.; Kawazu, A. *Mol. Cryst. Liq. Cryst. Sci. Technol. Sect. A* **1994**, *247*, 185.

(30) Macpherson, J. V.; Unwin, P. R.; Hillier, A. C.; Bard, A. J. Unpublished results.

chemically active area was in the region 0.5−1 mm^2 (assuming linear diffusion and an irreversible process).[31]

Images of the dissolving surface were obtained in the contact mode under constant force conditions, where the integral and proportional gains had values of 4.0 and 7.0, respectively. The tip−sample force was minimized before imaging by reducing the set-point to a value just prior to tip disengagement. Images were acquired at set times post application of a 1-s potential pulse to the working electrode from +0.5 V, where no electrode reaction occurred, to either +0.9, +1.1, or +1.3 V, so as to initiate the electrolysis of bromide to tribromide at the working electrode.

Materials. Solutions were made up in acetonitrile (far-UV grade, BDH, Poole, England, or HPLC grade, EM Science, Gibbstown, NJ) and contained 0.05 M $LiClO_4$ (Aldrich, ACS reagent). These solutions were saturated with KBr (Fisons, A. R. reagent, U.K.), [KBr] = 6.5 × 10^{-3} M, as determined by measuring the steady-state transport-limited current for the oxidation of bromide to tribromide at a 25-μm-diameter Pt UME. The diffusion coefficient, D, of Br^- under these conditions was 1.25 × 10^{-5} cm^2 s^{-1}, from UME potential step chronoamperometry,[32] in excellent agreement with previously reported values.[33]

The potassium bromide single crystal was in the form of a cube of side 1 cm, grown from the melt (Crystran, Poole, U.K.), and the (100) cleavage face served as the substrate. The crystal was cleaved with a carbon steel blade immediately prior to use.

Results and Discussion

SECM Measurements. Linear sweep voltammetry for the oxidation of bromide at a Pt UME in acetonitrile solution, recorded over the potential range of 0.5 to 1.8 V vs AgQRE at a rate of 0.01 V s^{-1}, gave two clearly defined waves. The first wave ($E_{1/2}$ = 1.05 V vs AgQRE) corresponds to the oxidation of bromide to the acetonitrile stable tribromide species, while the second wave ($E_{1/2}$ = 1.42 V vs AgQRE) is due to the oxidation of tribromide to bromine.[33,34] Both waves showed a substantial degree of irreversibility on the voltammetric time scale of these measurements, in agreement with previous work.[34]

The determination of dissolution kinetics via SECM requires that the tip response for the electrochemical process of interest is well-defined in the absence of interfacial kinetic complications.[23−27] Chronoamperometric characteristics for the oxidation of bromide to tribromide at a Pt UME, measured after stepping the potential from open circuit to +1.3 V, revealed that this was a simple diffusion-controlled process[35] on a time scale of 400 μs and longer for UMEs with an electrode radius a = 2.5 μm. Moreover, when this process was carried out in the SECM configuration with a series of tips (a = 2.5, 5.0, and 12.5 μm) placed at distances, d, in the range 0.1a to 1.3a from an inert glass surface, diffusion-controlled (negative feedback) responses were observed to be in good agreement with theoretical predictions.[36] A typical steady-state approach curve for a Pt tip with a = 2.5 μm is shown in Figure 2a. The measured currents, i, have been normalized with respect to the steady-state current, $i(\infty)$, which flowed when the tip was placed far from the glass surface. Clearly the experimental data are in excellent agreement with the theory for this probe, which had an insulator to electrode diameter ratio, RG,[36] of 15.

When the glass surface was replaced with the (100) face of a freshly cleaved potassium bromide single crystal, the SECM chronoamperometric response for the oxidation of bromide to tribromide, which serves to induce the dissolution of KBr by creating a local undersaturation in the gap between the tip and the crystal face, was found to be in excellent agreement with the theory for diffusion-controlled dissolution of a binary (1:1) salt under conditions where only one ion-type in the solution is depleted and none of the lattice ions are buffered.[23] A typical approach curve of long time normalized current versus tip−crystal separation obtained with the smallest electrode employed (a = 2.5 μm), i.e., on the fastest time scale accessible, is shown in Figure 2b. The experimental data, shown alongside theory for a diffusion-controlled dissolution process, relate to a measurement time, t, of 32 ms (dimensionless time, $\tau = tD/a^2$ = 6.4). The normalized current ratio in this case is much higher than that for the inert glass surface because the local depletion of bromide ions by electrolysis at the tip electrode induces dissolution from the crystal surface. The effect of this process, outlined in more detail elsewhere,[23−27] serves to enhance the flux of bromide ions to the tip compared to the situation where the substrate is inert and electroactive material is transported to the electrode by hindered diffusion alone.[22,36a] It is clear that the dissolution process is effectively diffusion-controlled even at a probe−crystal separation as close as 400 nm (d/a = 0.16). As suggested previously, when these conditions are met, the minimum effective heterogeneous dissolution rate constant,[23] in terms of a first−order process, can be estimated from:

$$k' > 100D/a > 5 \text{ cm s}^{-1} \quad (1)$$

demonstrating that the dissolution kinetics are extremely rapid.

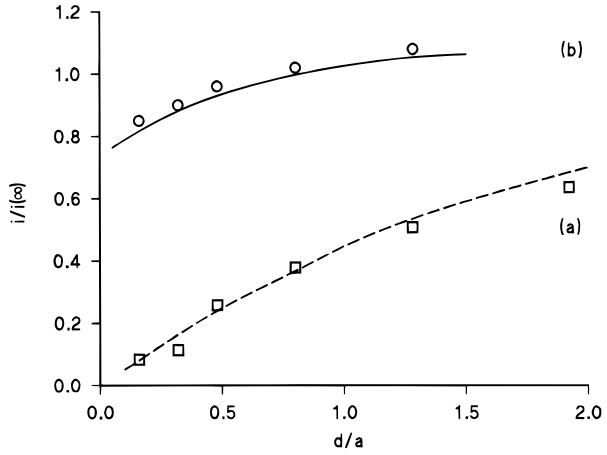

Figure 2. Steady-state approach curves of the diffusion-limited current for the oxidation of Br^- at a Pt tip (a = 2.5 μm) as a function of distance from a glass surface (□) and the (100) face of KBr (○). The theoretical behavior for (a) negative feedback (- - -) and (b) a diffusion−controlled dissolution process (−) under the conditions of the SECM measurements is also shown.

Integrated Electrochemical/AFM Probe Results. The sputtering technique used to create the integrated electrochemical AFM probe produced a tip and cantilever that were uniformly coated with metal. The presence of metal at the apex of the AFM tip was verified by measuring the tip−sample resistance as the tip was brought into contact with a conductive sample.[37] A small (10−50 mV) bias was applied between the Pt-coated AFM tip and a gold or graphite surface across a current limiting resistor (5 MΩ). As the tip−sample separation was reduced, the tip deflection and the tip−sample resistance were recorded

(31) Bard, A. J.; Faulkner, L. R. *Electrochemical Methods*; Wiley: New York, 1980; p 165.

(32) Denuault, G.; Mirkin, M. V.; Bard, A. J. *J. Electroanal. Chem.* **1991**, *308*, 27.

(33) Mussini, T.; Faita, G. In *Encyclopedia of Electrochemistry of the Elements*; Bard, A. J., Ed; Marcel Dekker: New York, 1973; Vol. 1, p 81.

(34) Iwasita, T.; Giordano, M. C. *Electrochim. Acta* **1969**, *14*, 1045.

(35) Theory is given in: Shoup, D.; Szabo, A. *J. Electroanal. Chem.* **1982**, *140*, 237.

(36) (a) Kwak, J.; Bard, A. J. *Anal. Chem.* **1989**, *61*, 1221. (b) Bard, A. J.; Denuault, G.; Friesner, R. A.; Dornblaser, B. C.; Tuckerman, L. S. *Anal. Chem.* **1991**, *63*, 1282.

(37) O'Shea, S. J.; Atta, R. M.; Welland, M. E. *Rev. Sci. Instrum.* **1995**, *66*, 2508.

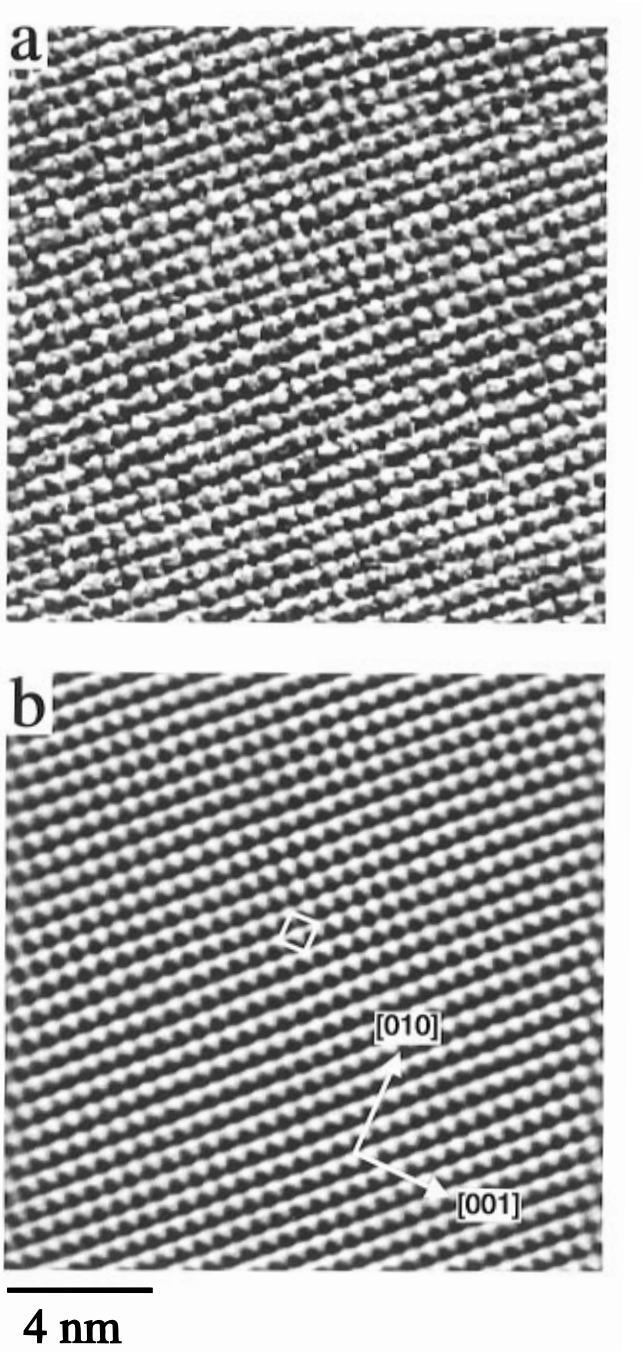

Figure 3. High-resolution AFM image of the (100) face of the KBr surface in an acetonitrile solution saturated with KBr: (a) raw data; (b) filtered data. The unit cell is depicted with measured lattice constants of $a_1 = a_2 = 7.1 \pm 0.4$ Å.

simultaneously. For most tips, the resistance dropped at contact between tip and sample, indicating the presence of conductive material at the tip apex.

The imaging ability of the Pt-coated AFM probe appeared unaffected by the presence of the additional metal layer. With this probe, steps with heights of atomic dimension (*vide infra*) and high-resolution lattice images of the (100) face of the KBr surface were easily resolved in an acetonitrile solution saturated with KBr. Figure 3 illustrates a representative AFM image taken at high resolution on the (100) face of KBr with the Pt-coated AFM probe. The periodic registry of this surface is clear in both the raw (Figure 3a) and filtered (Figure 3b) data. The observed periodicity is typical of previously published images of the KBr surface in vacuum[28] and depicts a rectangular unit cell with lattice constants $a_1 = a_2 = 7.1 \pm 0.4$ Å, which correspond to the [100] and [010] lattice directions and compare favorably to those determined by X-ray diffraction ($a_{[100]} = a_{[010]} = 6.6$ Å).

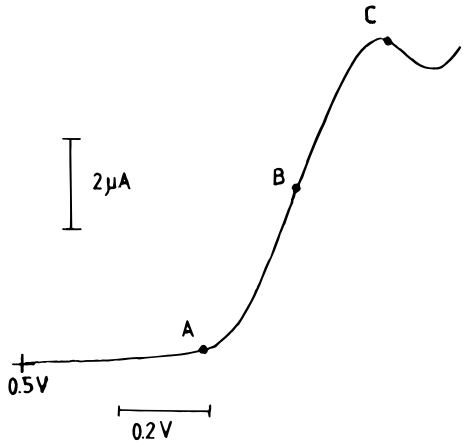

Figure 4. Linear sweep voltammogram at a Pt-coated AFM probe for the oxidation of Br^- to Br_3^- in an acetonitrile solution saturated with KBr and with 0.05 M $LiClO_4$ as a supporting electrolyte. The potential scan rate was 0.05 V s^{-1}. The potentials to which the probe was pulsed during electrochemically induced AFM dissolution studies are also indicated.

A typical linear sweep voltammogram for the oxidation of bromide to tribromide at a Pt-coated AFM probe, recorded at a scan rate of 0.05 V s^{-1}, is shown in Figure 4. This measurement was made with the KBr sample retracted far from the tip (~100 μm), to ensure that the electrode diffusion field would not be significantly perturbed by the sample and to suppress the induction of dissolution. Together, the results in Figures 3 and 4 demonstrate that high-resolution topographical and electrochemical measurements are feasible at the Pt-coated AFM probe.

As noted above, a consequence of the procedure adopted to electrically insulate the AFM probe is that the tip and a significant fraction of the cantilever are electrochemically active. Thus, most of the electrochemically active part of the probe (apart from the apex of the tip in contact with the surface) is at a sufficiently great distance from the crystal surface (3−40 μm) to ensure that the dissolution images reported below relate to effective conditions of a diffusion-controlled process.

Figure 5 shows a sequence of in-situ AFM images of an area of the KBr surface recorded prior to (Figure 5a) and after (Figure 5b,c) electrochemically inducing dissolution by pulsing the probe potential from +0.5 to +0.9 V (point A in Figure 4) for 1.0 s and then back to +0.5 V. The step to +0.9 V (just into the bromide−tribromide oxidation wave) slightly depletes the bromide concentration, providing the thermodynamic force for dissolution, but the irreversibility of the electrochemical process dictates that tribromide is not reduced back to bromide when the potential is returned to +0.5 V.

Although the solution in contact with the crystal surface was nominally saturated with KBr before dissolution was induced, Figure 5a clearly shows the presence of a dissolution spiral, which was found to slowly rotate over a period of several minutes, consistent with a very slowly dissolving surface. The spiral comprises widely spaced steps (width in the range of 400−900 nm) of about unit cell height (3.4 ± 0.5 Å) winding down to an origin located at the lower left of Figure 5a. The spiral is not of the classical archemedian type,[19,38] as a result of a number of breaks in the steps. As identified below, these breaks coincide with the cores of other dislocations which emerge at the surface.

(38) Frank, F. C. *Discuss. Faraday Soc.* **1949**, *48*, 67.

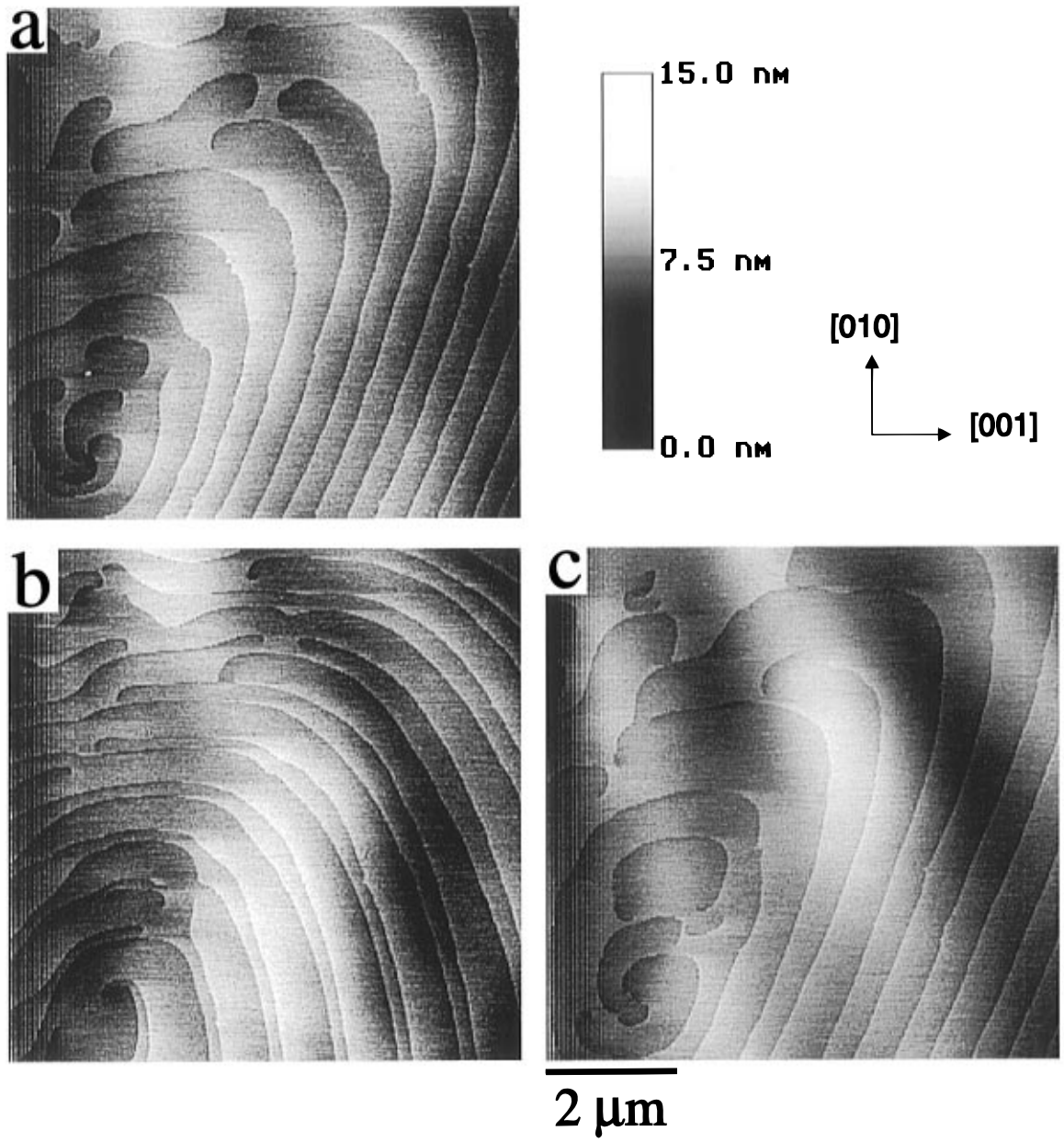

Figure 5. AFM images of a 7 μm $\times$ 7 μm area of the (100) face of potassium bromide in contact with a saturated KBr solution (a) prior to, (b) 60 s after, and (c) 8 min after the application of a 1-s potential pulse (+0.5 to +0.9 V) to the electrochemically-active AFM probe.

The wide spacing of the steps far from the origin of the main spiral is diagnostic of only very slightly undersaturated solution.[39] Even though dissolution is not electrochemically induced during the recording of the image in Figure 5a, a slowly dissolving surface is not unexpected, since small temperature increases in the sample chamber can arise from the diode laser in the detection unit.[40] The influence of the scanning tip may also create slightly undersaturated conditions as a result of local frictional heating. These effects were minimized by periodically injecting fresh solution into the reaction cell, but nonetheless, even small variations in temperature will lead to slightly undersaturated (or supersaturated) conditions sufficient to promote dissolution (or growth) at highly strained dislocation features. Although rotating spirals have been monitored interferometrically at lower resolution in situ on growing potassium phthalate[41] and cadmium iodide[42] crystal surfaces and in AFM growth studies of calcite,[43] protein crystals,[44] and organic charge transfer salts,[45] Figure 5a represents the first direct in-situ observation of the operation of this mechanism for the dissolution of an ionic crystal surface in contact with a liquid medium.

The surface 60 s after electrochemically initiating the dissolution process is shown in Figure 5b. The predominant dissolution spiral is seen to be double armed, resulting in step pairing around the dislocation core. The step height across the double arm is typically 6.7 $\pm$ 0.5 Å. The resulting decrease in the distance between steps as they pair indicates that the step velocity and hence dissolution rate has increased from the initial conditions (Figure 5a), where only thermal perturbations from equilibrium provided the driving force for dissolution of the surface. Spirals with two arms which rotate together as the step

(39) Cabrera, N.; Levine, M. M. *Philos. Mag.* **1956**, *1*, 450.
(40) Kipp, S.; Lacmann, R.; Schneeweiss, M. A. *Ultramicroscopy* **1995**, *57*, 333.
(41) Van Der Hoek, B.; Letten, L. A. M. J.; Enckevort, W. J. P. *J. Cryst. Growth* **1983**, *62*, 603.
(42) Tsukamoto, K. *J. Cryst. Growth* **1983**, *61*,199.
(43) Gratz, A. J.; Hillner, P. E.; Hansma, P. K. *Geochim. Cosmochim. Acta* **1993**, *57*, 491.
(44) Durbin, S. D.; Carlson, W. E.; Saros, M. T. *J. Phys. D: Appl. Phys.* **1993**, *26*, B128.
(45) Hillier, A. C. Ph.D. Thesis, University of Minnesota, 1995.

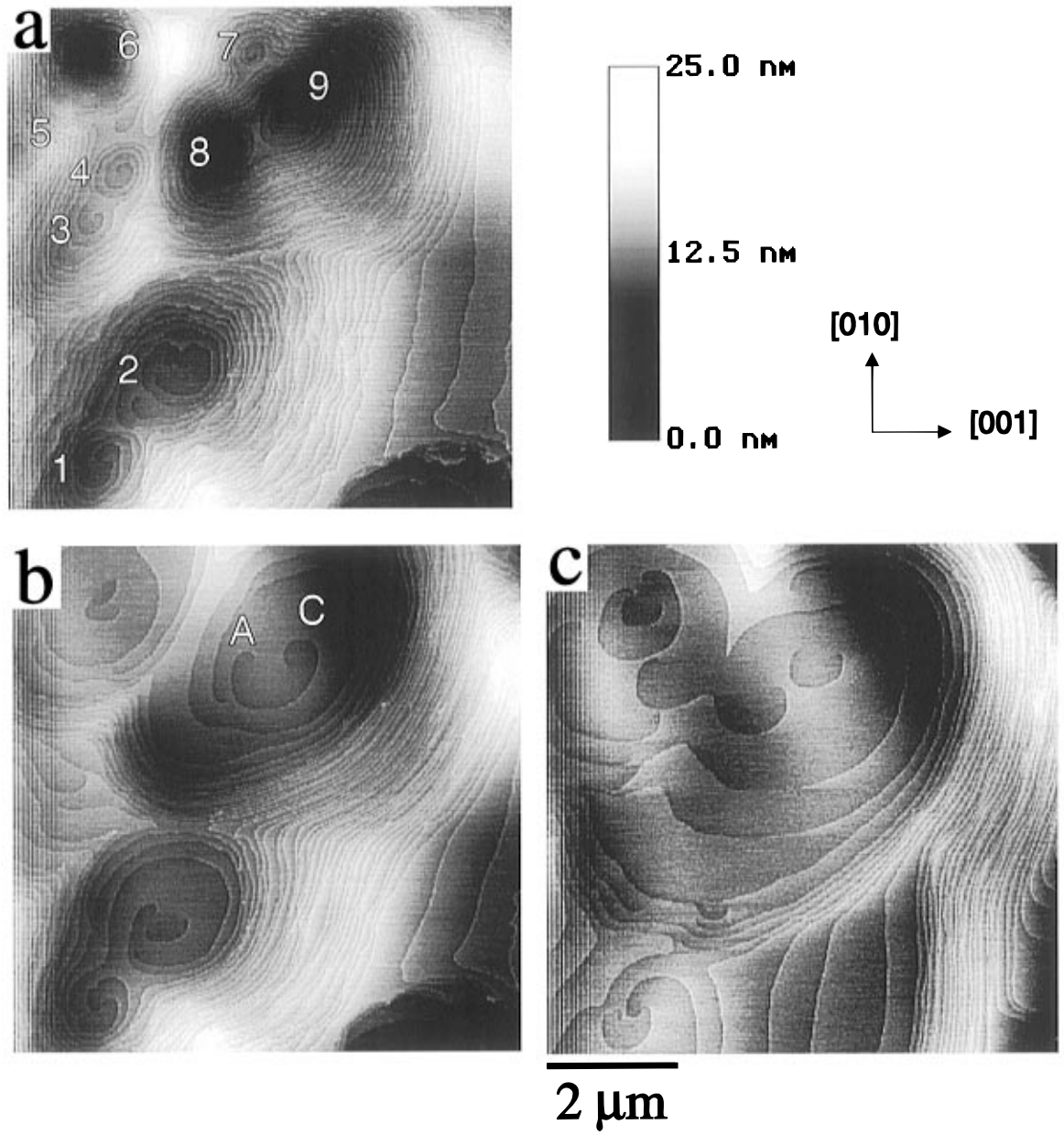

Figure 6. AFM images of the same area of the KBr (100) face as in Figure 5 immediately after the application of a 1-s potential pulse (+0.5 to +1.1 V) to the electrochemically-active probe. The images were recorded sequentially at a rate of 21 s/frame. Clockwise (c) and anticlockwise (a) rotating spirals are identified in (b).

advances have recently been observed by AFM during the growth of inorganic[43] and organic crystals[44] but Figure 5b is the first example of a double-armed spiral imaged dynamically on a dissolving surface. For the KBr crystal lattice, the observation of such a spiral suggests that the screw dislocation at the origin is characterized by a Burgers vector of two unit cells. Since the strain energy density associated with a dislocation is a function of the square of the Burgers vector,[46] this observation provides a plausible explanation of why this dislocation, and no other, dominates in the imaged region when the solution is very close to saturation. Figure 5c was recorded 8 min after the initial 1-s potential pulse and demonstrates that, as the solution returns to equilibrium through dissolution of the crystal, the dissolution rate decreases, resulting in an increase in step spacing and a return to a stable surface structure similar to that depicted in Figure 5a.

The evolving topography of the crystal surface following a 1-s potential pulse further into the Br^- to Br_3^- oxidation wave, from +0.5 to +1.1 V (point B in Figure 4), is depicted in Figure 6. These images clearly demonstrate that, under conditions of high mass transport rates, dissolution still occurs via a spiral mechanism, but many more dislocations are activated and hence revealed. In total, nine spirals appear in the area of the surface under study (Figure 6a). Coupled with Figure 5, this observation of the spiral mechanism underpins a number of the theoretical treatments of crystal dissolution.[1,47] Although this model was originally introduced by Burton, Cabrera, and Frank[19,38] to describe the growth of metals from a vapor, it has been adapted and used widely to interpret experimental dissolution kinetics,[1,47] including the rapid kinetics deduced in previous SECM studies.[23−26] The results herein provide the first in-situ evidence of the validity of this mechanism in describing fast dissolution processes of ionic single crystal surfaces. The difference in the shape and depth of the features in Figure 6a again suggests different strain energies associated with the core dislocations, with the deepest spirals associated with the largest strain energy.[46]

(46) Sangwal, K. *Etching of Crystals*; Elsevier Science Publishers: North Holland, Amsterdam, 1987, and references therein.

(47) Zhang, Z.; Nancollas, G. H. *Rev. Mineral.* **1990**, *43*, 365.

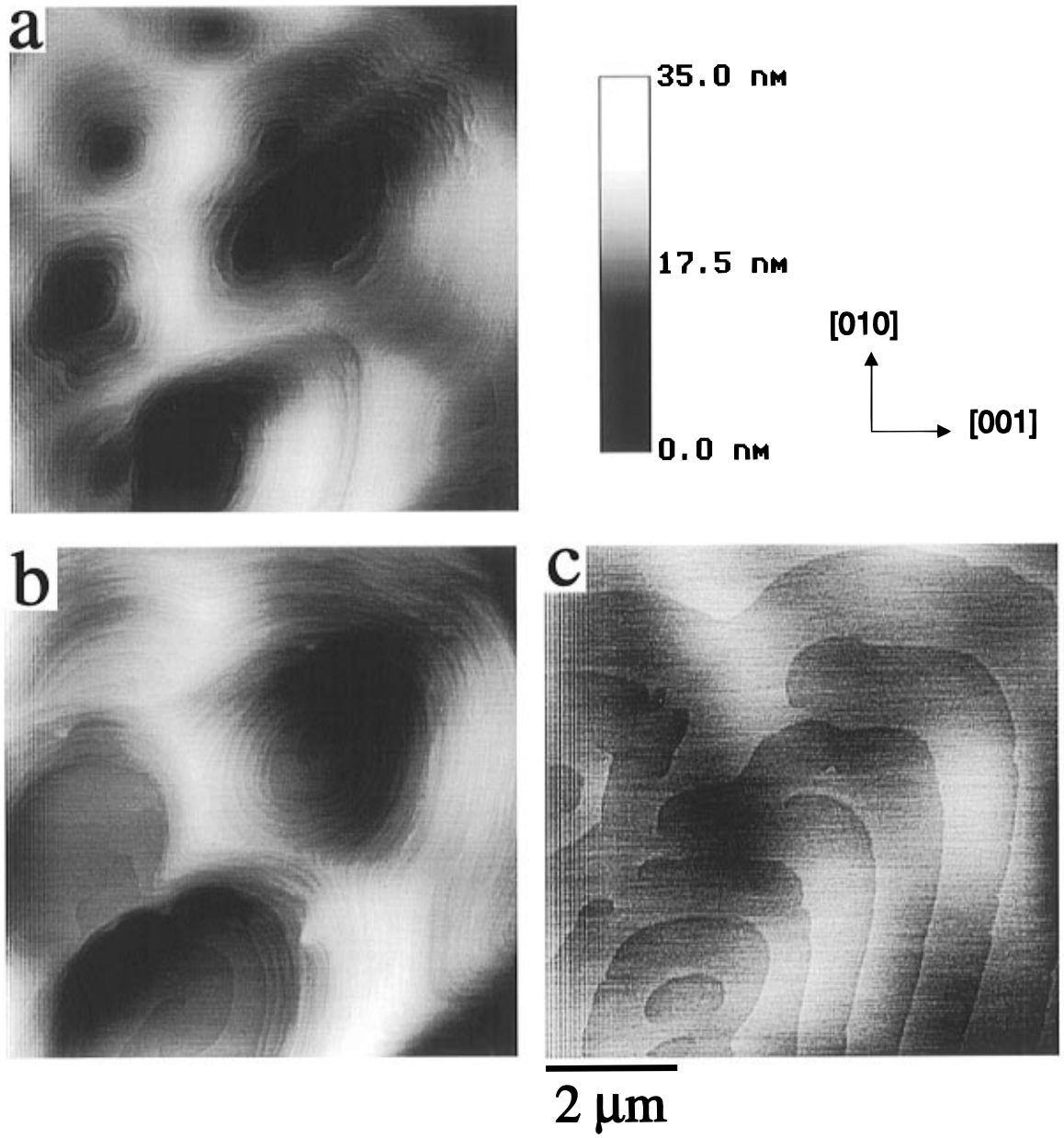

Figure 7. AFM images of the same area of the KBr (100) face as in Figure 5: (a) Immediately after the application of a 1-s potential pulse (+0.5 to +1.3 V) to the electrochemically-active AFM probe, (b) ca. 60 s later, and (c) ca. 180 s later.

The operation of the spiral dissolution process is consistent with the SECM kinetic results, which demonstrated that the dissolution process will be predominantly transport-controlled over a wide range of mass-transport rates, including those of the AFM experiments. However, the geometry of the electrochemically active AFM probe is such that there will be a variation in the electrode−crystal separation. Thus the mass-transport rate may vary over the region of interest during dissolution. In the case of an SECM-induced transport-controlled dissolution process involving one species, the transport rate, and hence the rate of dissolution, increases as the tip−sample gap decreases (see refs 24−27). This situation is akin to positive feedback. For the system of interest here, which involves two species (K^+ and Br^-), the buildup of electroinactive species (K^+) in the tip−sample gap serves to flatten the approach curve (Figure 2b). The dissolution rate in this case is not as sensitive to tip−substrate separation, but cannot be completely overlooked. Nevertheless, under these conditions the dissolution process is sufficiently rapid to maintain the crystal/solution interfacial region close to effectively saturated conditions, thereby disfavoring alternative dissolution mechanisms, such as birth and spread processes,[48,49] which require a large interfacial undersaturation.

Although the crystal/solution interface remains close to saturation during electrochemically-induced dissolution, the electrolysis process creates a significantly undersaturated zone in the solution adjacent to the probe and, crucially, in the gap between the probe and the surface. In the period following the application of the potential pulse, the solution returns to a saturated state through continued dissolution of the crystal surface, as evident from the images in Figure 6b,c. These images provide vital information on how steps of unit cell height associated with specific dislocations retreat during dissolution. Evidently, further dissolution normal to the surface slows considerably and continued dissolution occurs via the motion of steps away from the dislocation core, resulting in the step spacing becoming wide toward the center of the spiral and closer at a distance from the core (Figure 6c). Spirals with this morphology have been predicted theoretically for dissolution

(48) Ohara, M.; Reid, R. C. *Modeling Crystal Growth Rates from Solution;* Prentice Hall: Englewood Cliffs, NJ, 1973, and references therein.
(49) Bennema, P. *J. Cryst. Growth* **1984**, *69*, 182.

processes close to saturation.[50] Ex-situ optical microscopy studies of the surfaces of naturally-occurring hematite crystals have also identified spirals of this type[51] on a much larger scale, but the natural dissolution conditions are difficult to predict,[52] making quantitative interpretation difficult.

The images in Figure 6 contain information on the influence of etching conditions on step orientations for the KBr (100) surface. Under conditions of fast dissolution (far from equilibrium), just after the potential step (Figure 6a), dissolution produces surface steps that, near the dislocation core, are isotropic with no preferred orientations, as expected for a crystal dissolution or growth process controlled by solution diffusional processes. As the rate of surface etching slows and the crystal dissolution process approaches equilibrium, surface steps facet along the directions of lowest surface energy corresponding to the strongest crystallographic bonding directions.[53] In AFM, the influence of a finite tip scan rate has been observed to obscure the apparent orientation of moving steps, particularly when the step velocity is comparable or faster than the tip scan rate.[8,12] However, under conditions where the tip scan rate exceeds the step velocity, as in Figure 6c, the observed orientation reflects the actual step direction. Analysis of Figure 6c (see also Figure 5) demonstrates that the steps favor an orientation along the [010] and [001] crystallographic directions at slow etch conditions. These orientations correspond to the direction of strong Coulombic bonding between neighboring K^+ and Br^- sites[28] in the lattice.

Figure 6b,c also demonstrates elegantly the interactions between closely spaced spirals at the points where they intercept. Note the step pattern that results from the interception of spirals which rotate in opposite directions, labeled A (anticlockwise rotation, moving outward from the center) and C (clockwise rotation) in Figure 6b. The steps emerging from dislocations A and C travel toward one another and annihilate when they intersect, leaving a single step connecting the dislocation cores, the morphology of which is very similar to that predicted theoretically for this situation by Burton, Cabrera, and Frank.[19]

After several minutes the surface was found to reconstruct to a form which was similar to that which prevailed prior to the induction of dissolution. A subsequent 1-s pulse of the probe potential from 0.5 to 1.3 V (point C in Figure 4) and back to 0.5 V was then applied to increase the transport driving force exerted on the dissolution process. Figure 7a was recorded immediately after the pulse and demonstrates that the same dislocations are revealed as in Figure 6a. However, the spirals penetrate deeper into the crystal surface, as expected for a diffusion-controlled process under more extensive dissolution conditions due to a faster mass-transfer rate from the crystal surface. As described above, the solution returns to a saturated state via the further dissolution of the crystal surface, which can be followed over time. Figures 7b and 7c show the surface about 60 and 180 s, respectively, after the potential pulse, demonstrating that the surface reconstructs to a morphology which is very similar to that prior to all of the induced dissolution measurements, depicted in Figure 5a.

Conclusions

The development of an integrated electrochemical/AFM probe has allowed the surface processes which accompany dissolution from the (100) face of a single crystal of KBr to be monitored in real time under defined conditions identified from SECM kinetic measurements. It has been established that the diffusion-controlled dissolution process of the (100) face of KBr in acetonitrile solution occurs via a spiral mechanism. Many of the surface dynamics observed during dissolution by this experimental approach are consistent with classical dissolution models. More generally, the AFM approach described opens up a new method of inducing and monitoring reactions at electrically insulating surfaces. For dissolution reactions in particular, electrochemical control of the interfacial conditions and extent of reaction diversifies the range of surface activities that are accessible to study by AFM.

Acknowledgment. We thank the EPSRC for an equipment grant to P.R.U. (GR/H63739) and an earmarked studentship to J.V.M. A.J.B. acknowledges the National Science Foundation and the Robert A. Welch Foundation. This work has been facilitated by a NATO collaborative research grant (CRG 941226), which we gratefully acknowledge.

JA960842R

(50) Van Der Hoek, B.; Van Der Eerden, J. P.; Bennema, P.; Sunagawa, I. *J. Cryst. Growth* **1982**, *58*, 365.
(51) Sunagawa, I.; Bennema, P. *J. Cryst. Growth* **1981**, *53*, 490.
(52) Sunagawa, I. *Am. Mineral.* **1962**, *47*, 1332.
(53) Ideas of this type have been put forth, for example, in the periodic bond chain,[54] surface roughening,[55] and attachment energy models.[56]
(54) Hartman, P.; Perdok, W. *Acta Crystallogr.* **1955**, *8*, 49, 521, 525.
(55) Bennema, P. *J. Phys. D: Appl. Phys.* **1993**, *26*, B1.
(56) (a) Hartmann, P.; Bennema, P. *J. Cryst. Growth.* **1980**, *49*, 145. (b) Berkovitch-Yellin, Z. *J. Am. Chem. Soc.* **1985**, *107*, 8239.